ORIGINAL ARTICLE

CrossMark

Contact Model of Revolute Joint with Clearance Based on Fractal Theory

Shi-Hua Li[*], Xue-Yan Han, Jun-Qi Wang, Jing Sun and Fu-Juan Li

Abstract

The contact stiffness of a mechanical bonding surface is an important parameter in determining the normal and radial contact force. To improve the calculation accuracy of the contact force model, the surface roughness of the bonding surface and the energy loss that necessarily occurs during the impact process should be considered comprehensively. To study the normal contact force of a revolute joint with clearance more accurately in the case of dry friction, a nonlinear stiffness coefficient model considering the surface roughness was established based on fractal theory, which considers the elastic, elastic-plastic, and plastic deformations of the asperities of the contact surface during the contact process. On this basis, a modified nonlinear spring damping model was established based on the Lankarani–Nikravesh contact force model. The laws influencing the surface roughness, recovery coefficient, initial velocity, and clearance size on the impact force were revealed, and were compared with the Lankarani–Nikravesh model and a hybrid model using MATLAB. The maximum impact force was obtained using a modified contact force model under different initial velocities, different clearances, and different degrees of surface roughness, and the calculated results were then compared with the experiment results. This study indicates that the modified model can be used more widely than other models, and is suitable for both large and small clearances. In particular, the modified model is more accurate when calculating the contact force of a revolute joint with a small clearance.

Keywords: Fractal theory, Modified contact model, Surface roughness, Lankarani–Nikravesh model

1 Introduction

In recent years, many scholars domestically and abroad have conducted a number of studies on the contact impact problem of dynamics with clearance. A common contact theory is the Hertz contact theory [1]; however, this theory can only describe the elastic deformation of the material during the contact process, and does not consider the energy dissipation. A contact force model with nonlinear damping (Hunt–Crossley model) was thus proposed by Hunt et al. [2], which considers the dissipation of energy during the contact process. Yan et al. [3] introduced the application of a clearance model in the analysis of nonlinear characteristics, a performance evaluation, and a reliability evaluation of the mechanical system dynamics. Han et al. [4] used the joint contact impact force as a

parameter to achieve a high-precision lifetime prediction of a mechanism. Lankarani et al. [5] determined the relationship between the damping factor and restitution coefficient by analyzing the energy loss in a system before and after the contact process, and then put forward the Lankarani–Nikravesh continuous contact force model (L–N model). The L–N model not only considers the dissipation of energy during the contact process, but also reflects the influence of the material properties, geometric characteristics, and motion states of the contact body during the contact process. Based on the L–N model and improved elastic foundation contact model [6], a hybrid model was established by Bai et al. [7], through which the nonlinear stiffness coefficient was presented. Wang et al. [8] established an improved nonlinear contact impact force model by considering the axial dimensions, material coefficients, and energy loss comprehensively. However, the previous modeling methods were all established at a macro level, and do not reflect the microscopic characteristics

*Correspondence: shli@ysu.edu.cn
Parallel Robot and Mechatronic System Laboratory of Hebei Province, Yanshan University, Qinhuangdao 066004, China

Li *et al. Chin. J. Mech. Eng.* (2018) 31:109

Page 2 of 11

of the contact surface, such as the influence of the micro topography and surface roughness on the contact stiffness.

There are numerous micro-convex bodies on an actual motion pair surface, all of which have a particular degree of roughness. A rough surface morphology has an important influence on the contact stiffness coefficient [9, 10], and affects the contact impact force during an actual contact collision. Therefore, drawing on research methods regarding the contact problems of the surface morphology, a contact model of a revolute joint with clearance when considering the surface morphology can be established, which is significant to a precision analysis and dynamic design of the mechanical system dynamics.

In fact, many asperities appear on a rough contact surface, and a rough surface morphology has an important influence on [11]. Scholars have conducted a number of studies on theoretical contact force models over the years, including the classic GW model [12], WA model [13], and MB model [14]. Furthermore, taking account of the influences of the surface asperities grade, the deformation characteristic, and the contact area, Yuan et al. [15, 16] established and analyzed the fractal contact mode between rough surfaces based on the fractal theory. Pan et al. [17, 18] derived a theoretical three-dimensional mechanical joint surface based on the W-M function of the three-dimensional joint surface topography. Liu et al. [19] established a fractal model of the tangential contact stiffness of two spherical surfaces when considering the friction factors. Wang et al. [20] established a deterministic model for the elastoplastic contact of rough surfaces under combined loads, and obtained the actual contact area, pressure distribution, and plastic deformation of the micro-convex peaks. A series of studies were carried out on the model of the contact stiffness coefficient of the contact surface. However, there have been relatively few studies establishing the organic connections between the macroscopic levels and microscopic states when considering a rough surface.

In this paper, the contact stiffness coefficient was derived when considering the surface roughness of the contact surface, and a modified contact force model was obtained. Based on the fractal theory, a modified normal contact stiffness coefficient model was also established, which considers the contact surface roughness, as well as the elastic, elastic-plastic, and plastic deformations of the asperities during the contact process. Meanwhile, a modified contact force model was established by combining the L–N model expression. Finally, an experimental system was developed, and the correctness of the model was verified through an experimental study.

2 Establishment of Modified Contact Force Model

When two surfaces consisting of asperities are close to each other, the contact only occurs at the top of the asperity owing to the asperities on the contact surface of the actual motion joint. During a study on the surface contact, the contact of two surfaces is usually simplified using the contact between a rough surface and a rigid plane [21].

2.1 Contact Deformation of Asperity

Based on fractal theory, the distribution function of asperity on contact surface $n(a')$ [22] is given as

$$\begin{cases} n(a') = \left| \frac{dN}{da'} \right| = \frac{D-1}{2} \cdot \varphi^{(3-D)/2} \cdot \frac{a_l'^{(D-1)/2}}{a'^{(D+1)/2}} & (2 < D < 3) \\ \varphi^{(3-D)/2} - 1 + \varphi^{-(D-1)/2(D-3)/(D-1)} = \frac{3-D}{D-1} & (2 < D < 3) \\ A_r = \frac{D-1}{3-D} \cdot \varphi^{(3-D)/2} \cdot a_l' \end{cases} \tag{1}$$

where parameter D is the fractal dimension, φ is the domain extension factor for the asperity size distribution, a' is the area of a contact spot, a_l' is the area of the largest contact spot, and A_r is the real area of contact.

According to the results in Refs. [23, 24], the critical deformation δ_c and the elastic and plastic deformations demarcated by the critical area a_c' are given by

$$\begin{cases} \delta_c = \frac{2^{D-7}\pi^{(5-D)/2}}{G^{2-D}(\ln\gamma)^{1/2}} \left(\frac{KH}{E} \right)^2 \cdot a'^{(D-1)/2}, \\ a_c' = \left[\frac{2^{11-2D}}{9\pi^{4-D}} G^{2D-4} \ln\gamma \left(\frac{E^*}{H} \right)^2 \right]^{1/(D-2)}, \end{cases} \tag{2}$$

where parameter G is a characteristic length of scale of the surface; K is the correlation coefficient [25], which is usually 2.8; H is the hardness of softer materials; and γ is a constant, which is usually 1.5. The composite elastic modulus E^* is given by

$$\frac{1}{E^*} = \frac{1-v_i^2}{E_i} + \frac{1-v_j^2}{E_j}, \tag{3}$$

where parameter v is the Poisson ratio.

Three deformation stages may occur on the asperity of a rough surface during the contact process, namely, elastic deformation, elastic-plastic deformation, and complete plastic deformation stages.

If $\delta \leq \delta_c$, the asperity is an inelastic deformation. Therefore, the elastic load P_e on such an asperity, and the contact area of asperity a, are given by the Hertz theory [24] as follows:

$$\begin{cases} a_e = \pi R \delta, \\ P_e = \frac{4}{3} E R^{1/2} \delta^{3/2}. \end{cases} \tag{4}$$

The range of elastic plastic deformation zone is derived as $\delta_c \leq \delta \leq 110\delta_c$ [26, 27]. This stage can be divided into

Li *et al.* Chin. J. Mech. Eng.   (2018) 31:109

Page 3 of 11

two stages: the first stage of elastic-plastic deformation $(\delta_c \leq \delta \leq 6\delta_c)$ and the second stage of elastic-plastic deformation $(6\delta_c \leq \delta \leq 110\delta_c)$. In the elastic-plastic deformation stage, the normal load and contact area of asperity can be written as

$$
\begin{cases}
a_{ep1} = 0.93\pi R \cdot \dfrac{\delta^{1.136}}{\delta_c^{0.136}}, \\[2mm]
a_{ep2} = 0.94\pi R \cdot \dfrac{\delta^{1.146}}{\delta_c^{0.146}}, \\[2mm]
P_{ep1} = \dfrac{2}{3}KH\pi R \times 1.03\dfrac{\delta^{1.425}}{\delta_c^{0.425}}, \\[2mm]
P_{ep2} = \dfrac{2}{3}KH\pi R \times 1.40\dfrac{\delta^{1.263}}{\delta_c^{0.263}}.
\end{cases}
\tag{5}
$$

If $\delta > 110\delta_c$, the asperity is a plastic deformation. Therefore, the normal load P_p and the contact area of asperity a_p are given by

$$
\begin{cases}
a_p = a', \\
P_p = Ha'.
\end{cases}
\tag{6}
$$

2.2 Modified Contact Stiffness Model

The ratio of contact force increment to contact distance variation is defined as the contact stiffness, and therefore the stiffness of the asperity under various stages of deformation can be obtained as follows:

$$
\begin{cases}
k_{ne} = \dfrac{dF_e}{d\delta} = \dfrac{4-D}{3-D} \cdot \dfrac{2^{15}E^*}{3\pi^{0.5}} \cdot a'^{1/2}, \\[3mm]
\qquad k_{nep1} = \dfrac{1.03}{3} \times \left(\dfrac{3.7 - 0.85D}{3-D} \right) \\[3mm]
\cdot \dfrac{2^{0.15D+0.675}E^{*0.85}KH^{0.15}G^{0.3-0.15D}}{\pi^{0.075D+0.2}\ln\gamma^{0.075}} \cdot a'^{0.075D+0.35}, \\[3mm]
\qquad k_{nep2} = \dfrac{1.4}{3} \times \left(\dfrac{1.526 - 0.263D}{3-D} \right) \\[3mm]
\cdot \dfrac{2^{0.474D-0.107}E*^{0.526}KH^{0.474}G^{0.948-0.474D}}{\pi^{0.273D-0.448}(\ln\gamma)^{0.237}} \cdot a'^{0.237D+0.026}.
\end{cases}
\tag{7}
$$

The total stiffness between the contact surfaces only occurs during the elastic deformation stage, that is, the sum of the stiffness of the three stages of the elastic deformation, the first stage of the elastic-plastic deformation, and the second stage of the elastic-plastic deformation. Therefore, the normal total stiffness between the contact surfaces K_n is given by

$$
\begin{aligned}
K_n &= \int_{a'_c}^{a'_l} k_{ne} n(a')da' + \int_{\left(\frac{1}{6}\right)^{\frac{1}{D-2}}a'_c}^{a'_c} k_{nep1} \\
&\quad + \int_{\left(\frac{1}{110}\right)^{\frac{1}{D-2}}a'_c}^{\left(\frac{1}{6}\right)^{\frac{1}{D-2}}a'_c} k_{nep2} n(a')da' \\
&= \varphi^{(3-D)/2} \cdot \big\{ g_1 \cdot (mA_r)^{(D-1)/2}\big[(mA_r)^{(2-D)/2} - a'^{(2-D)/2}_c \big] \\
&\quad + g_2 \cdot (mA_r)^{(D-1)/2} \cdot g_3 + g_4(mA_r)^{(D-1)/2} \cdot g_5 \big\},
\end{aligned}
\tag{8}
$$

where

$$
g_1 = \frac{2\sqrt{2}E}{3\sqrt{\pi}} \cdot \frac{4-D}{3-D}\frac{D-1}{2-D},
$$

$$
\begin{aligned}
g_2 &= \frac{1.03 \times 2^{0.15D+0.675}K^{0.15}H^{0.15}G^{0.3-0.15D}E^{*0.85}}{1.275\ln\gamma^{0.075}\pi^{0.075D+0.2}} \\
&\quad \cdot \frac{(D-1)(1.85 - 0.425D)}{(3-D)(2-D)},
\end{aligned}
$$

$$
g_3 = a_c'^{0.425(2-D)}\left[1 - \left(\frac{1}{6} \right)^{-0.425} \right],
$$

$$
\begin{aligned}
g_4 &= \frac{1.4 \times 2^{0.474D+1.107}K^{0.474}H^{0.474}G^{0.948-0.474D}E^{*0.526}}{0.789(\ln\gamma)^{0.237}\pi^{0.237D-0.448}} \\
&\quad \cdot \frac{(D-1)(1.526 - 0.263D)}{(3-D)(2-D)},
\end{aligned}
$$

$$
g_5 = a_c'^{0.263(2-D)}\left[\left(\frac{1}{6} \right)^{-0.263} - \left(\frac{1}{110} \right)^{-0.263} \right],
$$

$$
m = \frac{3-D}{D-1}\varphi^{2/3(3-D)}.
$$

It can be seen from the formula that the contact stiffness K_n varies with the actual contact area A_r. In fact, the actual contact area A_r should be less than the nominal contact area A. Thus, an area proportion coefficient λ of less than 1 is found, and the relationship between the actual contact area and the nominal contact area can be described as

$$
A_r = \lambda A
$$

where λ is assumed as an invariable constant during the contact process.

According to the improved elastic foundation model [7], a pin is equivalent to a rigid wedge. The analytical model for the revolute joints with clearance is illustrated in Figure 1.

The relationship between semi-angle contact ε and the penetration displacement u can be expressed as follows:

$$
\cos\varepsilon = \frac{\Delta R}{\Delta R + u},
\tag{9}
$$

where parameter ε is the semi-angle contact, u is the penetration displacement, and R_1 and R_2 refer to the radii of the pin and the hole in the plate, respectively. Here, $\Delta R = R_2 - R_1$ represents the radial clearance of the joints.

Because ΔR is much less than R_1 and R_2, the relationship between l and ε can be expressed as

$$
l = 2R_2 \sin\left(\frac{\varepsilon}{2} \right),
\tag{10}
$$

where the parameter l is the length of the chord.

Li *et al. Chin. J. Mech. Eng.* (2018) 31:109
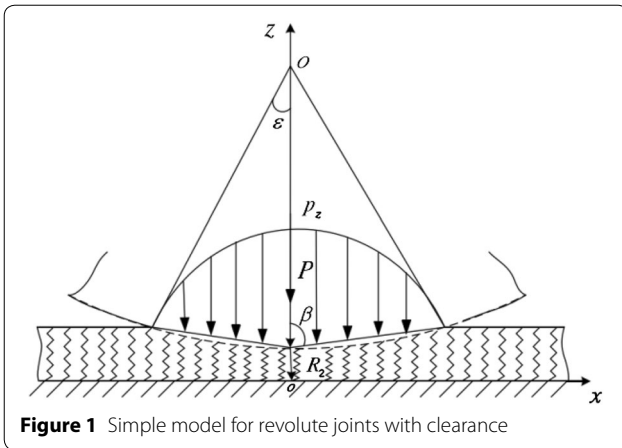
Page 4 of 11

Figure 1 Simple model for revolute joints with clearance

If the axial length is b, the nominal contact area A can be expressed as

$$A = lb = 2R_2 b \sqrt{\frac{u}{2(\Delta R + u)}}, \tag{11}$$

The relationship between the modified stiffness coefficient and the compression depth u can be obtained through formulae (8) and (11) as

$$K_n = \varphi^{(3-D)/2} \cdot \left\{ g_1 \cdot \left(s \left(\frac{u}{2(\Delta R + u)} \right)^{1/2} \right)^{(D-1)/2} \left[\left(s \left(\frac{u}{2(\Delta R + u)} \right)^{1/2} \right)^{(2-D)/2} - a_c'^{(2-D)/2} \right] \right. \\ \left. + g_2 \cdot g_3 \cdot \left(s \left(\frac{u}{2(\Delta R + u)} \right)^{1/2} \right)^{(D-1)/2} + g_4 \cdot g_5 \cdot \left(s \left(\frac{u}{2(\Delta R + u)} \right)^{1/2} \right)^{(D-1)/2} \right\}. \tag{12}$$

In addition, the fractal dimensions D and G [22] are given as

$$D = \frac{1.54}{R_a^{0.045}} + 1, \tag{13}$$

$$G = 10^{-\frac{5.26}{R_a^{0.045}}}. \tag{14}$$

2.3 Modified Contact Force Model

The L–N model [28, 29] considers the energy dissipation during the contact process, the expression of which is as follows:

$$F_n = Ku^n + D_n \dot{u}, \tag{15}$$

where parameter K is the stiffness coefficient, and D_n is the damping coefficient.

In this paper, based on the L–N model expression, the fractal contact force model is established by replacing

the stiffness coefficient K with the modified stiffness coefficient K_n, and is written in the following form:

$$F_n = K_n u^n + D_n \dot{u}, \tag{16}$$

3 Numerical Simulation of Modified Contact Force Model

Using the modified model proposed in this paper, a one-shot contact was analyzed.

3.1 Simulation Parameters of the Mechanism

The material and size parameters of the shaft and sleeve were taken as follows: $E = 207$ GPa, $\nu = 0.3$, $\sigma_v = 335$ MPa, $m = 1$ kg, $b = 0.01$ m, and $R_2 = 0.01$ m.
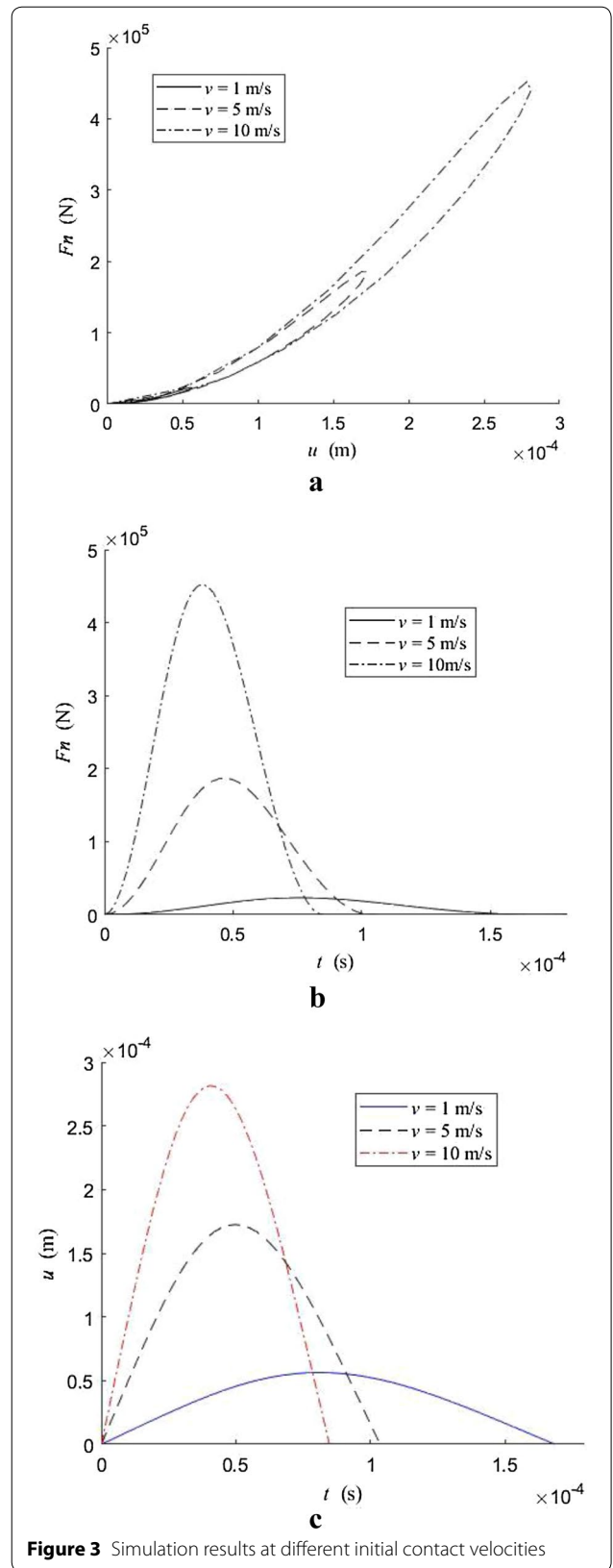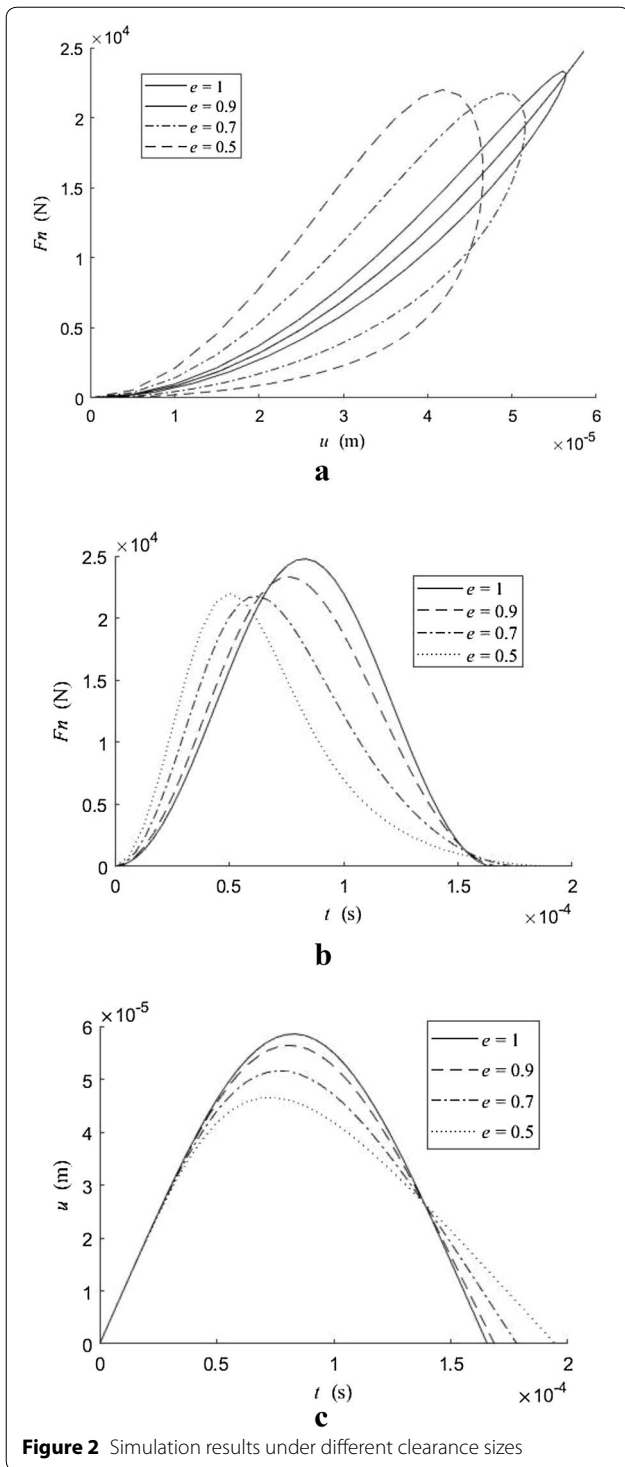
Because the L–N and hybrid models [6] do not take the roughness of the contact surface into account, roughness Ra in the modified model has a smaller value of 0.05 for unifying the parameters.

With the increase in contact load, the real contact area tends to be a fixed value; however, this value is less than the nominal contact area (approximately 5–10% of the nominal contact area) [30–34]. Therefore, the area proportion coefficient λ in this paper can be valued at 0.05.

3.2 Analysis of Contact Process under Different Restitution Coefficients

Assume that the size of the clearance is 0.5 mm, the initial contact velocity is 1 m/s, and the restitution coefficient is different. The simulation results of the modified model are shown in Figure 2.

Figure 2(a) shows the characteristics of damping hysteresis during the contact process. The damping of the material will cause a loss of energy, and the restitution coefficient will be smaller, whereas the loss of energy during the contact process will be larger. The modified contact force model presented in this paper can better describe the loss of energy during the contact process when the restitution coefficient is small. Furthermore, Figure 2(b) and (c) also conform to the change in contact force and deformation during actual contact. Therefore, it is possible to describe the contact process with different restitution coefficients.

Li *et al.* Chin. J. Mech. Eng.   (2018) 31:109

Page 5 of 11

Figure 2 Simulation results under different clearance sizes

Figure 3 Simulation results at different initial contact velocities

Li *et al. Chin. J. Mech. Eng.* (2018) 31:109

Page 6 of 11

3.3 Analysis of Contact Process at Different Initial Velocities

Assume that the clearance size is 0.5 mm, the restitution coefficient is 0.9, and the initial contact velocity differs. The simulation results of the modified model are as shown in Figure 3.

It can be seen from Figure 3 that, with an increase in the initial contact velocity, the contact force and deformation increase rapidly, and the contact time is shortened, which is consistent with the actual contact process. In addition, when the contact force is at maximum, the deformation also reaches the maximum value, which is consistent with the theoretical formula.

3.4 Analysis of Contact Process for Different Amounts of Roughness

Assume that the clearance size is 0.5 mm, the restitution coefficient is 0.9, and the initial contact velocity is 1 m/s. The simulation results of the modified model when choosing different amounts of contact surface roughness are as shown in Figure 4.

As Figure 4 shows, the roughness of the contact surface is smaller, the contact force is larger, and the time to reach the maximum contact force is shorter. Moreover, the roughness is smaller, as is the maximum deformation; in addition, the time to reach the maximum deformation is also shorter, the reason for which is that a smaller amount of contact surface roughness leads to a larger fractal dimension, and a larger stiffness coefficient. When the initial conditions are the same, the stiffness is larger, the contact force is greater, and the deformation is smaller.

4 Comparative Analysis of Models

In this paper, a single contact simulation of the L–N model and the hybrid model established in Ref. [6] was carried out, and the results were compared with those of the modified model.

4.1 Comparative Analysis of Models under Different Clearance Sizes

Assume that the restitution coefficient is 0.9, the initial contact velocity is 1 m/s, and the clearance size is different. The contact force of the three models varies with the amount of deformation, as shown in Figure 5.

As shown in Figure 5, the modified model shows a slight difference with the L–N and hybrid models with a large clearance, whereas the difference between the modified model and the hybrid model is greater than
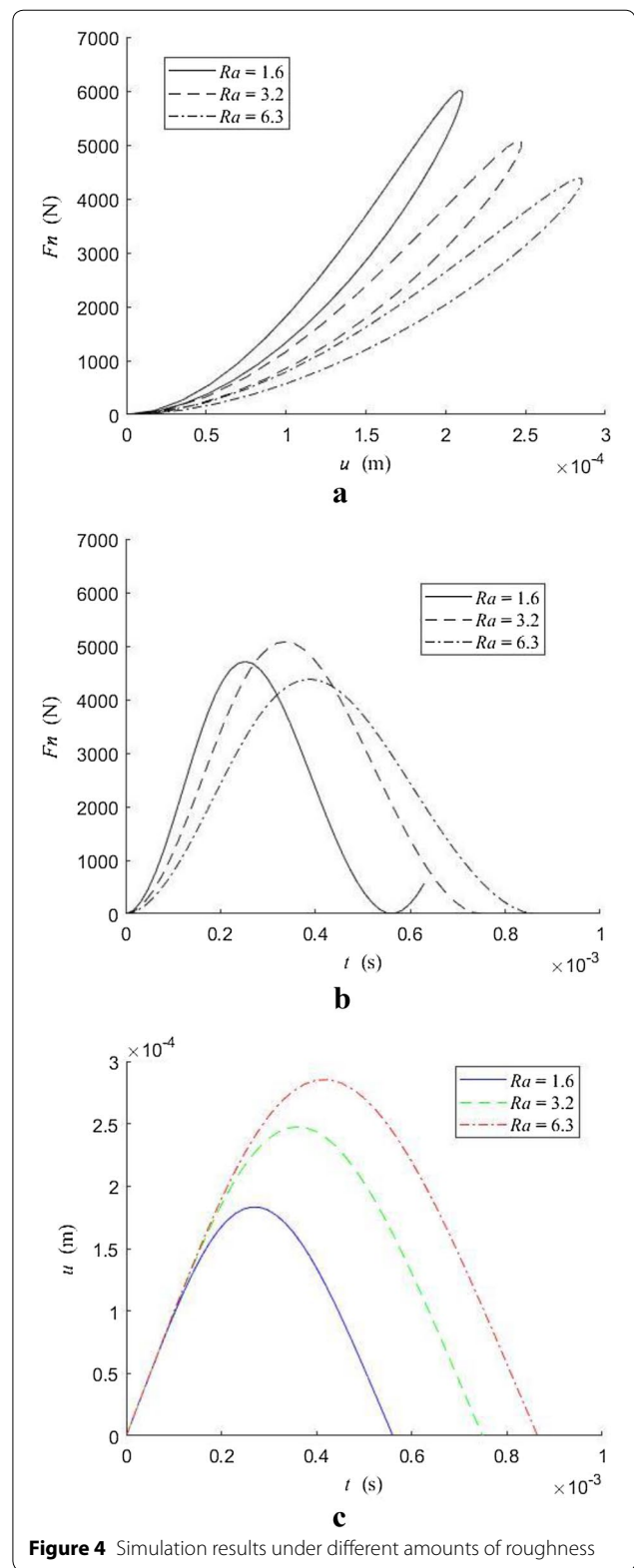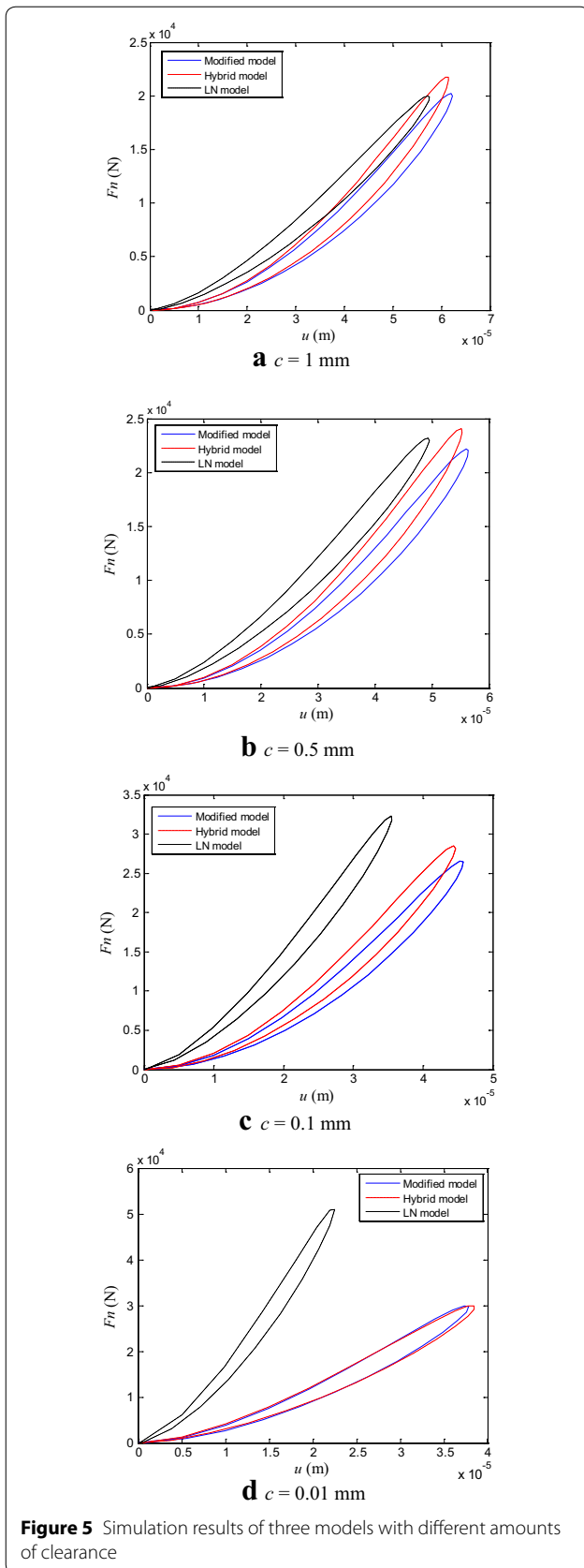

Figure 4 Simulation results under different amounts of roughness

Li *et al. Chin. J. Mech. Eng.*   (2018) 31:109

Page 7 of 11

Figure 5 Simulation results of three models with different amounts of clearance

that of the L–N model when the clearance decreases, the reason for which is that the L–N model is based on the Hertz contact theory, and is suitable for the case of non-coordinated contact with a large clearance. For a small clearance, the error in the calculation result is large. The modified model proposed in this paper and the hybrid model are suitable for both large and small clearances, and their calculation results are more accurate. In addition, when the clearance is small, the contact becomes closely conformal contact. Because the modified model described in this paper is based on the fractal theory and micro-surface topography, it is more accurate when calculating a small-clearance contact.

4.2 Comparative Analysis of Models under Different Restitution Coefficients

Assume that the clearance size is 0.5 mm, the initial contact velocity is 1 m/s, and the restitution coefficient is different. The contact force of the three models varies with the amount of deformation, as shown in Figure 6.

As shown in Figure 6, when the restitution coefficient is large, the calculated results of the three models are relatively similar, whereas when the restitution coefficient is small, the calculated results of the modified model in this paper are similar to those of the hybrid model, which is quite different from the L–N model. The damping force terms in the modified model and the hybrid model can reflect the loss of energy better during the contact process with a smaller restitution coefficient, thereby improving the calculation results. The modified contact force model has a broader range of application.
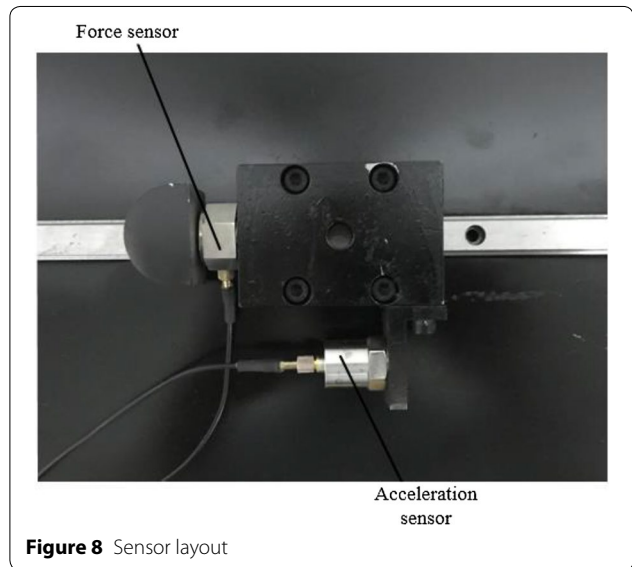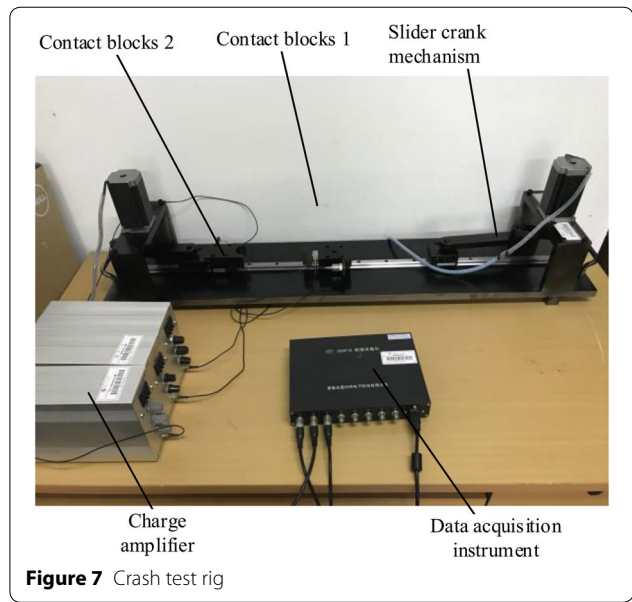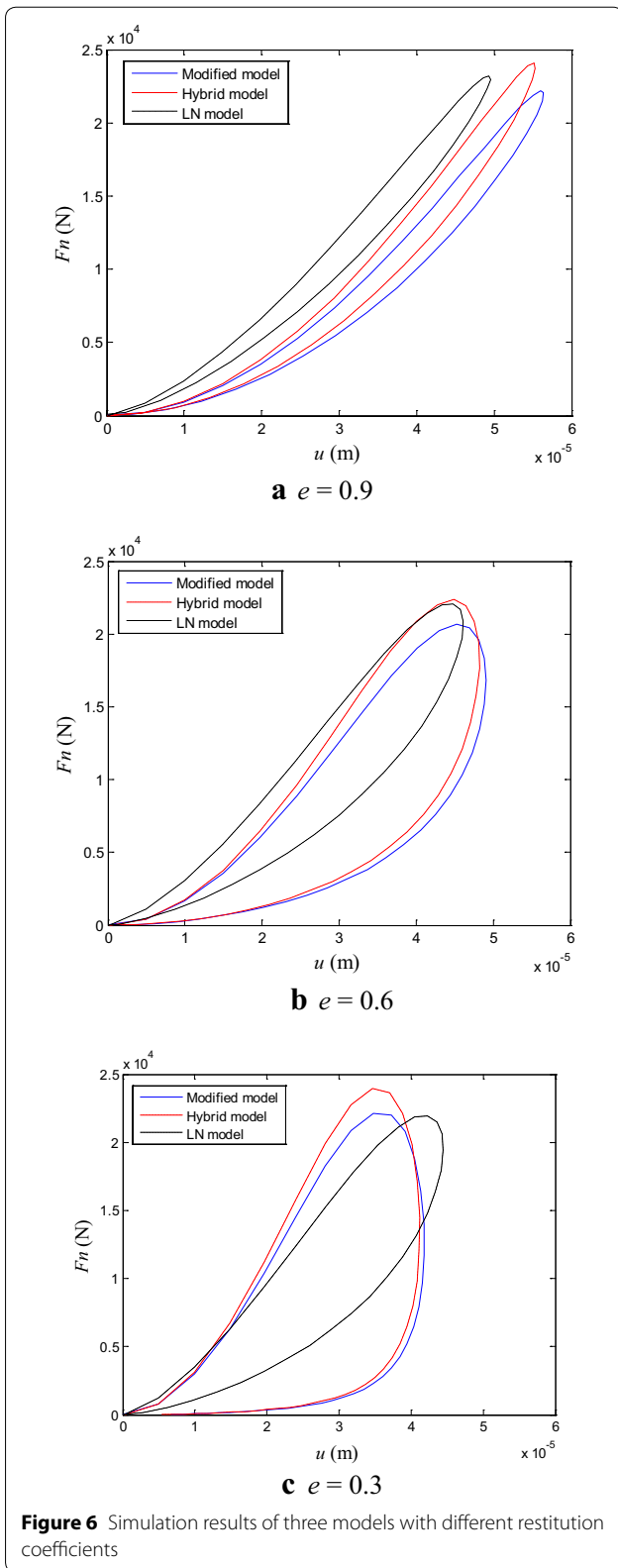
5 Experiment Verification

A crash test rig was designed, the results of which prove the correctness of the theoretical analysis.

5.1 Test Rig

The test rig is shown in Figure 7, which consists of a slider crank mechanism, a simulation contact part, and the data acquisition system. By controlling the speed of the motor, the slider crank mechanism can make contact block 1 obtain different initial velocities. The simulation contact part can simulate the contact between the shaft and sleeve when designing contact blocks 1 and 2 as convex and concave. The data acquisition system can transfer the signal of the test rig to the data acquisition instrument, and display it in a computer in real time.

During the experiment, contact block 1 was driven by the motor, and impacted contact block 2, which was fixed on the left end. As shown in Figure 8, the maximum contact force during the contact process was measured using

Li *et al. Chin. J. Mech. Eng.* (2018) 31:109

Page 8 of 11

Figure 6 Simulation results of three models with different restitution coefficients

a force sensor mounted on contact block 1, and the initial velocity during the contact process was measured using an acceleration sensor, also mounted on contact block 1. The measurement signal was then collected by the data

Figure 7 Crash test rig

Figure 8 Sensor layout

Table 1 Parameter values of the modified model

Parameter	Values	Parameter	Values
Elastic modulus	207 GPa	Equivalent mass	0.85 kg
Poisson ratio	0.3	Simulation clearance	0.5 mm
Surface roughness	6.3	Area scale coefficient	0.05
Convex radius	16.5 mm	Restitution coefficient	0.46

Table 2 Experimental measurements and numerical results

Experiment no.	Measured initial velocity (m/s)	Measured contact force (N)	Theoretical contact force (N)	Relative error
1	0.131	258.18	234.5	− 9.63%
2	0.150	308.53	281.6	− 9.56%
3	0.241	499.00	533.4	6.38%
4	0.299	711.06	708.6	− 0.42%
5	0.302	739.00	721.7	− 2.50%
6	0.351	935.00	881.4	− 6.08%
7	0.388	1089.17	1010	− 7.82%
8	0.400	1188.66	1087	− 9.29%
9	0.421	1250.00	1128	− 7.30%
10	0.427	1183.78	1150	− 2.87%
11	0.577	1661.07	1718	3.32%
12	0.630	2035.22	1924	− 5.77%
13	0.735	2205.81	2365	6.77%
14	0.818	2435.45	2703	9.91%
15	0.882	2827.45	2994	5.58%
16	0.970	3191.83	3391	5.90%
17	0.989	3347.17	3477	3.74%
18	1.044	3752.15	3722	− 0.80%
19	1.070	3812.87	3842	0.78%
20	1.110	3934.63	4039	2.60%

Table 3 Experimental measurements and numerical results for $c = 0.5$ mm and $R_a = 6.3$

Experiment no.	Measured initial velocity (m/s)	Measured contact force (N)	Theoretical contact force (N)	Relative error
1	0.131	258.18	242.4	− 6.1%
2	0.150	308.53	288.5	− 6.5%
3	0.241	499.00	530.3	6.3%
4	0.299	711.06	698.4	− 1.8%
5	0.302	739.00	707.2	− 4.3%
6	0.343	847.78	832.4	− 1.8%
7	0.388	1059.17	972.7	− 8.2%
8	0.411	1112.06	1048.0	− 5.8%
9	0.422	1128.54	1084.0	− 3.9%
10	0.427	1183.78	1100.0	− 7.1%
11	0.577	1661.07	1611.0	− 3.0%
12	0.624	1697.08	1778.0	4.8%
13	0.633	1748.96	1812.0	3.6%
14	0.735	2205.81	2188.0	− 0.8%
15	0.818	2435.30	2503.9	2.8%
16	0.882	2827.45	2755.8	− 2.5%
17	0.970	3191.83	3102.5	− 2.8%
18	0.989	3347.17	3177.4	− 5.1%
19	1.044	3752.15	3399.4	− 9.4%
20	1.070	3812.87	3508.7	− 8.0%
21	1.110	3934.63	3677.1	− 6.5%

Table 4 Experimental measurements and numerical results for $c = 1$ mm and $R_a = 3.2$

Experiment no.	Measured initial velocity (m/s)	Measured contact force (N)	Theoretical contact force (N)	Relative error
1	0.101	174.56	190.6	9.2%
2	0.127	249.63	256.2	2.6%
3	0.253	652.16	623.3	− 4.4%
4	0.262	624.69	651.8	4.3%
5	0.297	746.77	766	2.6%
6	0.305	822.75	792.8	− 3.6%
7	0.354	1044.31	959.2	− 8.1%
8	0.378	1011.05	1044.5	3.3%
9	0.383	1084.9	1062.3	− 2.1%
10	0.391	1130.68	1090.9	− 3.5%
11	0.392	1036.99	1094.4	5.5%
12	0.402	1197.2	1130.1	− 5.6%
13	0.419	1176.76	1190.7	1.2%
14	0.423	1163.02	1204.9	3.6%
15	0.448	1313.78	1297.7	− 1.2%
16	0.480	1448.97	1419.2	− 2.1%
17	0.484	1395.57	1434.5	2.8%
18	0.499	1580.81	1491.5	− 5.6%
19	0.534	1752.62	1624.7	− 7.3%
20	0.556	1744.38	1709.5	− 2.0%
21	0.602	1909.18	1896.4	− 0.7%
22	0.619	1992.19	1965.7	− 1.3%
23	0.649	2171.33	2088	− 3.8%
24	0.735	2647.09	2443.3	− 7.7%
25	0.809	2629.39	2767.3	5.2%
26	0.910	3074.65	3210.9	4.4%
27	0.911	3275.15	3215.3	− 1.8%
28	0.925	3320.92	3276.7	− 1.3%
29	0.926	3533.94	3281.1	− 7.2%
30	0.930	3009.95	3298.7	9.6%

acquisition instrument and the charge amplifier, and displayed in real time in the computer.

The initial contact velocity measured through the experiment is substituted into the modified model for a numerical calculation, and the other parameters of the modified model are as given in Table 1.

5.2 Experimental Results and Analysis

The experiment and numerical results are shown in Tables 2, 3, 4 for different speeds, amounts of surface roughness, and clearances. The experiment data are consistent with the theoretical data as shown in the following tables, which illustrates that the modified normal contact force model proposed in this article is correct. The causes of the error may be from (1) vibrations and

Li *et al. Chin. J. Mech. Eng.*   (2018) 31:109

Page 10 of 11

friction during the collision process, (2) the scale coefficient of the area in the modified model is not constant when impacting at different speeds.

6 Conclusions

(1) In this paper, the contact stiffness coefficient was optimized based on the fractal theory, and a modified contact force model was proposed.

(2) The change law of the contact force of the modified contact force model under different parameters was provided.

(3) The modified model can describe the contact process with different restitution coefficients, which is suitable for both large and small clearances, and has a wider range of application. Furthermore, the modified model is more accurate when calculating the impact force of a contact with a small clearance.

(4) The agreement between the simulation and experiment results shows that the modified contact force model proposed in this paper can be used to calculate the contact force better when considering the surface roughness, and can therefore provide a reference for the establishment of contact models.

Authors' Contributions
S-HL was in charge of the whole trial; X-YH wrote the manuscript; J-QW designed and debugged the experiment; JS and F-JL assisted with sampling and laboratory analyses, as well as implementation of the experiment and date processing. All authors read and approved the final manuscript.

Authors' Information
Shi-Hua Li, born in 1966, is currently a professor, PhD Tutor at *Parallel Robot and Mechatronic System Laboratory of Hebei Province, China*. He received his PhD degree in *Yanshan University, China*, in 2004. His research interests include nonlinear dynamics and precision of spatial mechanism, the ory and application of parallel robot, micro-operation and micro-electromechanical systems.

Xue-Yan Han, born in 1978, is currently a PhD candidate at *Parallel Robot and Mechatronic System Laboratory of Hebei Province, China*. He received his master degree in *Yanshan University, China,* in 2007.

Jun-Qi Wan, born in 1993, is currently a master candidate at *Parallel Robot and Mechatronic System Laboratory of Hebei Province, China*.

Jing Sun, born in 1989, is currently a PhD candidate at *Parallel Robot and Mechatronic System Laboratory of Hebei Province, China*. He received his bachelor degree in *Yanshan University, China,* in 2014.

Fu-Juan Li, born in 1985, is currently a experimentalist at *Parallel Robot and Mechatronic System Laboratory of Hebei Province, China*. She received her master degree in *Yanshan University, China,* in 2012.

Competing Interests
The authors declare that they have no competing interests.

Publisher's Note
Springer Nature remains neutral with regard to jurisdictional claims in published maps and institutional affiliations.

References
[1] H Hertz. Ueber die Berührung fester elastischer Körper. *Journal Für Die Reine Und Angewandte Mathematik*, 2006, 1882(92): 156–171.
[2] K H Hunt, F R E Crossley. Coefficient of restitution interpreted as damping in vibroimpact. *Journal of Applied Mechanics,* 1975, 42: 440–445.
[3] S Z Yan, W W K Xiang, T Q Huang. Advances in modeling of clearance joints and dynamics of mechanical systems with clearances. *Acta Scientiarum Naturalium Universitatis Pekinensis,* 2016, 52(4): 741–755. (in Chinese)
[4] X Y Han, S H Li, Y M Zuo, et al. Motion characteristics of pointing mechanism with clearance in consideration of wear. *Chinese Space Science and Technology*, 2018, 38(4): 51–61. (in Chinese)
[5] H M Lankarani, P E Nikravesh. A contact force model with hysteresis damping for impact analysis of multibody systems. *Journal of Mechanical Design*, 1990, 112: 369–376.
[6] Z F Bai, Y Zhao, Z G Zhao. Dynamic characteristics of mechanisms with joint clearance. *Journal of Vibration and Shock*, 2011, 30: 17–20.
[7] C S Liu, K Zhang, R Yang. The FEM analysis and approximate model for cylindrical joints with clearances. *Mechanism & Machine Theory*, 2007, 42: 183–197. (in Chinese)
[8] X P Wang, G Liu, S X Ma. Dynamic characteristics of mechanisms with revolute clearance joints. *Journal of Vibration and Shock*, 2016, 35(7): 110–115. (in Chinese)
[9] S H Wen, X L Zhang, M X Wu, et al. Fractal model and simulation of normal contact stiffness of joint interfaces and its simulation. *Transactions of The Chinese Society of Agricultural Machinery*, 2009, 40: 197–202. (in Chinese)
[10] S H Wen, Z Y Zhang, X L Zhang, et al. Stiffness fractal model for fixed joint interfaces. *Acta Automatic Mechanica Sinica*, 2013, 44(2): 255–260.
[11] X P Li, W Wang, M Q Zhao, et al. Fractal prediction model for tangential contact damping of joint surface considering friction factors and its simulation. *Journal of Mechanical Engineering*, 2012, 48(23): 46–50. (in Chinese)
[12] J A Greenwood, J B P Williamson. Contact of nominally flat surfaces. *Proceedings of the Royal Society of London,* 1966, 295: 300–319.
[13] D J Whitehouse, J F Archard. The properties of random surfaces of significance in their contact. *Proceedings of the Royal Society A*, 1971, 316: 97–121.
[14] A Majumdar, B Bhushan. Fractal model of elastic-plastic contact between rough surfaces. *Journal of Tribology*, 1991, 113: 1–11.
[15] L Gan, Y Yuan, K Liu, et al. Mechanical model of elastic-plastic contact between fractal rough surfaces. *Chinese Journal of Applied Mechanics*, 2016, 33(5): 738–743. (in Chinese)
[16] Y Cheng, Y Yuan, L Gan, et al. The elastic-plastic contact mechanics model related scale of rough surface. *Journal of Northwestern Polytechnical University*, 2016, 34(3): 485–492. (in Chinese)
[17] W J Pan, X P Li, M Y Li, et al. Three-dimensional fractal theory modeling of tangential contact stiffness of mechanized joint surface. *Journal of Vibration Engineering*, 2017, 30(4): 577–586.
[18] X P Li, Q Guo, J S Li, et al. Fractal prediction modeling and simulation on normal surface contact stiffness. *Chinese Journal of Construction Machinery*, 2016,14: 281–287. (in Chinese)

Li *et al. Chin. J. Mech. Eng.* (2018) 31:109

Page 11 of 11

[19] P Liu, Q Chen, H Fan, et al. Research on fractal model of TCS between spherical surfaces considering friction factor. *China Mechanical Engineering*, 2016, 27(20): 2773–2778. (in Chinese)

[20] D C Xu, J G Wang. On deterministic elastoplastic contact for rough surfaces. *Tribology*, 2016, 36(3): 371–379. (in Chinese)

[21] W Wang, J B Wu, W P Fu, et al. Theoretical and experimental research on normal dynamic contact stiffness of machined joint surfaces. *Journal of Mechanical Engineering*, 2016, 52(13): 123–130. (in Chinese)

[22] S Wang, K A Komvopoulos. A fractal theory of the interfacial temperature distribution in the slow sliding regime: Part I—Elastic contact and heat transfer analysis. *Journal of Tribology*, 2009, 116: 812–822. (in Chinese)

[23] Y Zhang. *The study on the modeling of contact stiffness and static friction factor*. Taiyuan: Taiyuan University of Science and Technology, 2014. (in Chinese)

[24] J L Liou. *The theoretical study for microcontact model with Variable topography parameters*. Taiwan, China: Cheng Kung University, 2006.

[25] S R Ge, H Zhu. *The fractal of tribology*. Beijing: China Machine Press, 2005. (in Chinese)

[26] X C Meng. *Fractal contact model and dynamic characteristics of fixed curved joint surface*. Shenyang: Northeastern University, 2013. (in Chinese)

[27] H L Tian, T M Chen, J H Zheng, et al. Contact analysis of cylindrical pair with parallel axes. *Journal of Xi'an Jiaotong University*, 2016, 50: 8–15. (in Chinese)

[28] J Ma, L Qian, G Chen, et al. Dynamic analysis of mechanical systems with planar revolute joints with clearance. *Mechanism and Machine Theory*, 2015, 94: 148–164. (in Chinese)

[29] Z F Bai, Y Zhao. Dynamics modeling and quantitative analysis of mylti-body systems including revolute joint. *Precision Engineering*, 2012, 36(4): 554–567. (in Chinese)

[30] G Wang, H Liu, P Deng. Dynamics analysis of spatial multiboby system with spherical joint wear. *Journal of Tribology*, 2015, 137: 1–10. (in Chinese)

[31] L Li, A J Cai, L G Cai, et al. Micro-contact model of bolted-joint interface. *Journal of Mechanical Engineering*, 2016, 52(7): 205–212. (in Chinese)

[32] Y H Chen, X L Zhang, S H Wen, et al. Research on continuous smooth exponential model of elastic-plastic contact and normal contact stiffness of rough surface. *Journal of Xi'an Jiaotong University*, 2016, 50: 58–67. (in Chinese)

[33] L G He, Z X Zhuo, J H Xiang. Normal contact stiffness fractal model considering asperity elastic-plastic transitional deformation mechanism of joints. *Journal of Shanghai Jiaotong University*, 2015, 49: 116–121. (in Chinese)

[34] X G Ruan, J Zhang, L Li, et al. A new micro contact model for the joint interface. *Manufacturing Technology & Machine Tool*, 2017, 5: 67–73. (in Chinese)